JOURNAL OF OPTOELECTRONICS AND ADVANCED MATERIALS, Vol. 11, No. 2, February 2009, p. 123 - 133

3-nitroaniline and 3-nitrophenol – A novel non linear optical material

V. KRISHNAKUMAR*, R. NAGALAKSHMI, K. OZGA[b], M. PIASECKI[a], I. V. KITYK[c], P. BRAGIEL[a]

Department of Physics, Periyar University, Salem – 636 011, India
[a]Institute of Physics, J.Dlugosz University Czestochowa, Poland
[b]Institute of Biophysics, Częstochowa Technological University, Armii Krajowej 36 A, Czestochowa, Poland
[c]Chemical Department, Silesian Technological University, ul. Strzody 9, Gliwice, Poland

Single crystals of co-crystallized 3-nitroaniline and 3-nitrophenol (3-NA: 3-NPh) have been grown from saturated solution (pH= 3.26) of the synthesized salt of 3-NA: 3-NPh by the slow evaporation technique at 30°C using a mixture of chloroform and petroleum ether as a solvent. The structural, vibrational and second-order nonlinear optical properties of the crystals were studied under application of the polarized UV-induced field. Besides the ab initio quantum chemical calculations have been performed at HF/6-31G (d) and time dependent DFT method level to derive first order hyperpolarizability. To compare an influence of the crystalline long-range ordering and of the applied effective electric field to the nonlinear optical susceptibilities additional calculations were performed for second order susceptibilities within the FLAPW method. Comparing the values of the second order optical susceptibilities and of the first order hyperpolarizabilites we estimate the role of long-range order intrinsic charged defect states in the observed processes. Moreover, possible increase of the susceptibilities due to applied vectorial fields is discussed. The performed measurements of the effective second harmonic generation for the 1320 nm fundamental wavelength show substantial dependence of the effective second-order susceptibilities versus the applied nitrogen laser field polarized along the z-crystallographic axes. We have also investigated the anisotropic features of the optical second harmonic generation.

(Received January 16, 2009; accepted February 23, 2009)

Keywords: Solution growth, X ray diffraction, Vibrational spectroscopy, Hyperpolarizability, Second harmonic generation

1. Introduction

The search for novel crystals with promising nonlinear optical properties is still a challenge for scientists. The theoretical methods of studying the relationship between structure and the non linear optical (NLO) susceptibilities may be a better solution before venturing into the physical growth of the crystals. The ab initio quantum chemical calculations were extensively applied for the computations of some essential non linear optical parameters. The extreme structural diversity and flexibility are some major advantages of growing organic crystals. Further, the second harmonic generation (SHG) efficiency of a non linear optical crystal is inherently dependent upon its structural features. On a molecular scale the extent of charge transfer across the NLO chromophores determines the efficiency of the SHG output [1,2] . As a result it would be valuable to probe and understand the packing motif of such an overwhelming bias in this class to choose a useful and general design tool for organic nonlinear optical crystal engineering. The majority of organic compounds exhibiting large SHG efficiencies are polarizable acentric molecules with a π-conjugated electron donor acceptor arrangement causing effective charge transfer [3,4]. The efficient organic crystals developed up to now are the derivatives of nitrobenzene and/or aniline. Orthorhombic modifications of *m*-nitroaniline (*m*-NA) and *m*-nitrophenol (*m*-NPh) crystals exhibit optical nonlinearity described by third rank polar tensors and it is interesting to verify potential of their non linear optical properties. One of pioneering strategy of cocrystallization was proposed by Cara C.Evans and coworkers [5]. The attractive structural features of the investigated crystals are: extension of π conjugation bonds, good planarity and strong electron donor to acceptor ratio at opposite ends of the molecule. These crystals also possess advantages of containing high density of chromophores and thermodynamic stability. The cocrystallization of two chromophores, effectively an acid and base, is a widely used approach to the design of materials for non linear optical activities [6,7] and this enhances the first order hyperpolarizabilities.

In the second part we present technology of crystal growth, control of their structure and vibrational spectra. Section 3 presents principal results concerning evaluations of second order susceptibilities obtained by Full potential Linearized Augmented Plane Wave (FLAPW) method (FLAPW) and hyperpolarizabilities evaluated by time dependent density functional (TDDFT) approach. Experimental results devoted to optical and non-linear optical data with appropriate discussion are given in the Section 4.

2. Experimental

2.1. Crystal growth

The scheme of synthesis of the investigated compound is outlined in Fig.1 (a). A solution of m-NA and m-NPh in a mixture of chloroform and petroleum ether was mixed at room temperature. 3-nitroaniline is a weak base that gains a proton in acidic solution and forms the salt of the respective acid. During the proton transfer reaction a proton is transferred from the electron donor group of 3-nitrophenol to the electron acceptor group of 3-nitroaniline. From the molecular structure of 3-NA: 3-NPh (Chemical formula $C_6H_7N_2O_2^+ : C_6H_4NO_3^-$), we infer that the main fragment of the crystal to provide enhanced NLO efficiency is due to the relatively delocalized electronic cloud of the OH group of 3-nitrophenol. Selection of suitable solvent and solubility equilibrium [8,9] are crucial for the growth of good quality single crystals. The solubility of 3-NA : 3-NPh was assessed at room temperature in different polar solvents such as methanol, ethanol, acetone or combination of these solvents. From our solubility studies, we find that the title compound exhibits good solubility in mixed solvent of chloroform and petroleum ether. Single crystals of 3-NA: 3-NPh have been grown from saturated solution (pH= 3.26) of the synthesized salt of 3-NA: 3-NPh by the slow evaporation technique at 30°C using a mixture of chloroform and petroleum ether as a solvent at fixed temperature bath with thermostability ($\pm$ 0.01° C). Pale yellow crystals of size 2.1 x 0.8 x 0.3 cm^3 have been obtained within 15-20 days and they are shown in Fig. 1(b). For better understanding of the structure of the particular molecular fragments incorporated into the crystallographic unit we present a fragment of crystallographic structure (see Fig. 1c) in the **ac** crystallographic plane, which shows orientation of the particular donor acceptor clusters with respect to the crystallographic axes and possible deviations from the in-plane phenyl groups.

2.2 XRD measurements

The crystal dimensions and the angle between the faces of crystal were measured using the Zwei Kreis reflection goniometer (P-stoe company, Hiedelberg, Germany). X-ray diffraction data were collected at room temperature on ENRAF NONIUS CAD 4 single crystal diffractometer with a local hardware program. The preliminary cell parameters were obtained from least squares of the (θ, χ, Φ) angular values of 36 reflections (θ range= 2.19 to 24.96) appropriately well centered on the diffractometer. The intensity of 1831 reflections were recorded in the range 2.19º to 24.96º, 1626 reflections of which (with $F_0>4\sigma(F_0)$) were regarded as observed. The intensity of one standard reflection, recorded for every 100 reflections showed no significant changes. The recorded data were restricted with respect to polarization and Lorentz effects. The obtained crystallographic data reveals that the compound crystallizes in orthorhombic structure with the space group $Pca2_1$ (suitable space group for non linear optical activities). The unit cell parameters are a(Å) = 19.347, b(Å)=6.595 c(Å)=4.970 and α(°) = β (°)=γ (°)= 90.The unit cell contains four $C_6H_7N_2O_2^+ : C_6H_4NO_3^-$ molecules (point group symmetry C_{2V}) and the cell volume is 634.2 $(Å)^3$. The specific ionization of charge-transfer type molecules such as nitroanilines shifts the principal electronic band edge towards blue wavelength because of the inherently less polarizable nature.

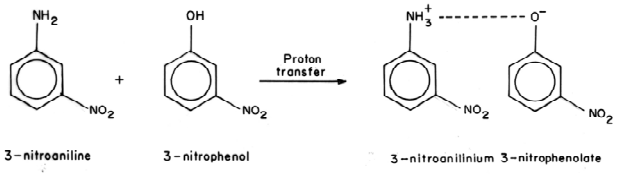

(a)

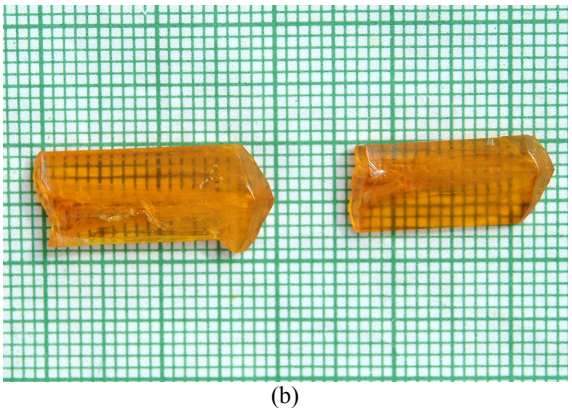

(b)

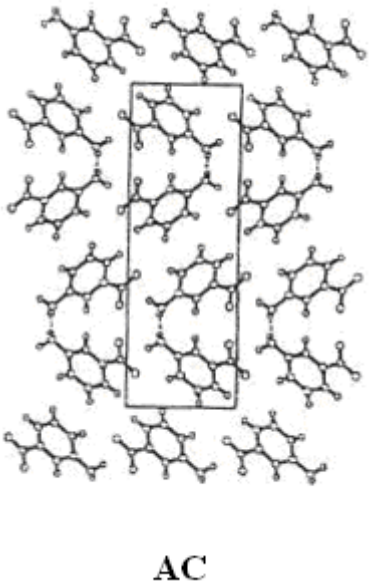

(c)

Fig 1. (a) Synthesis scheme, (b) 3-NA: 3-NPh crystal (c) Particular molecular fragments with crystallographic axes of the investigated crystal.

The selection of the anionic entity is crucial because it may determine total acentric architecture. Analysis of X-ray data of the investigated compound has shown the existence of polar chains as a common structural feature, supporting the assumption that N-H…..O (hydroxy) synthesis in nitroanilines and nitrophenols are so strong that they induce molecules to assemble in polar chains as the first aggregation step in solution, which in turn would induce the formation of acentric structures during the crystallization.

2.3 Recording of vibrational spectra

Polarized Raman and infrared spectra were recorded to interpret the bonding properties in the cocrystallized 3-NA: 3-NP single crystals. The mid Fourier transform infrared spectra of 3-NA: 3-NP were recorded at room temperature in the spectral range 400- 4000 cm^{-1} with spectral resolution of 4 cm^{-1} using Perkin Elmer FTIR, model SPECTRUM RX1 equipped with He–Ne laser source, KBr beam splitter and $LiTaO_3$ detector. The observed FTIR spectrum is given in Fig. 2. A well-grown single crystal was chosen and the crystallographic axes were determined using a polarizing microscope. The directions *x*, *y* and *z* of the crystal were chosen in accordance with crystallographic *a*, *b* and *c* axes. FT Raman spectrometer was used in the back scattering geometry (180° scattering). So the propagation direction of the exciting laser beam and that of the detected scattered radiation are collinear (opposite directions). The measurements were done with 4 cm^{-1} spectral resolution with the cw-laser operating at 100 mW power.

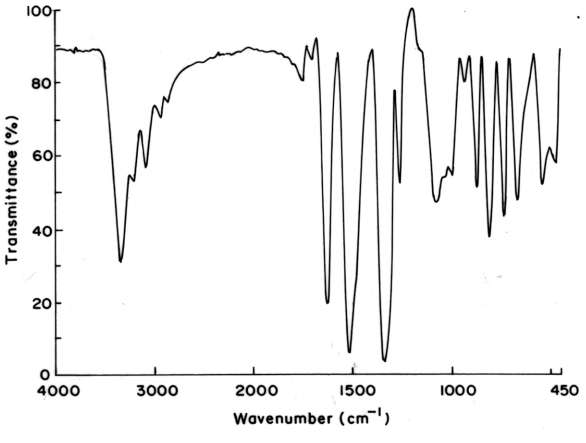

Fig 2. FTIR spectrum of 3-NA: 3-NPh crystal.

3. Calculations of first order hyperpolarizabilities and second-order optical susceptibilities

Hyperpolarizability computations were performed at the HF/ 6-31G (d) level using GAUSSIAN 98 W Program Package [12] for ionic pairs 3-NA and 3-NPh with electric field up to 4 kV/mm electric strength. The molecular geometry was optimized at the molecular dynamics MM+ force field method. The optimal configuration geometry is evaluated by minimizing the total energy with respect to all possible molecular conformation structural parameters without imposing molecular symmetry constraints. The first static hyperpolarizability (β_0) and its related properties (β, α_0 and $\Delta\alpha$) have been calculated using HF/6-31G(d) data within the finite field approach. In the presence of an applied dc-electric field, the energy of a system is a function of the electric field and the first hyperpolarizability (both static as well as frequency dependent) is a third rank tensor that can be described by a 3x3x3 matrix depending on applied dc electric strength. It is obvious that the lower part of the 3x3x3 matrices is a tetrahedral. The components of β are defined as the coefficients in the Taylor series expansion of the energy in the presence of external electric field factor. In this case the 27 tensor components of the 3D matrix can be reduced to 10 components because of the Kleinman symmetry conditions [13]. The matrix can be given in the lower tetrahedral format. When the external electric field is weak and homogeneous this expansion becomes

$$E = E^0 - \mu_\alpha F_\alpha - 1/2\ \alpha_{\alpha\beta} F_{\alpha\beta} - 1/6\ \beta_{\alpha\beta\gamma} F_\alpha F_\beta F_{\gamma+} \quad (1)$$

where E^0 is the energy of the unperturbed molecules. F_α is the strength of the electric field $\mu_{\alpha,}$ $\alpha_{\alpha\beta}$ and $\beta_{\alpha\beta\gamma}$ are the components of dipole moment, polarizabilities and first hyperpolarizabilities, respectively. The packing forces and intermolecular interactions in the crystal play a crucial part for the total experimentally observed macroscopic features of these crystals. Such intermolecular interactions may help to understand the origin of the macroscopically observed phenomena. The value of second order optical susceptibility $\chi^{(2)}$ in a given NLO system depends on the molecular hyperpolarizabilityβ, the number of chromophores and the degree of noncentrosymmetry.

Additionally the hyperpolarizabilities were calculated by TDDFT method. These calculations were performed by double zeta (DZ) Slater-type orbital basis set [14] and local density approximation (LDA) in which the exchange-correlation potential is a local functional of electron density. Core electrons as well as atomic positions were kept frozen within Born-Oppenheimer approach. The Broyden-Fletcher-Goldfarb-Shanoo method [15] was chosen to update Hessian matrix. The gradient convergence criterion was chosen to be 0.001 a.u./A which required to do 80 iterations. The excited states were calculated by TDDFT approach [16]. TDDFT approach usually provides a good accuracy for calculations of excitation energies, exceeding those from configuration interactions [17].

Additionally calculations reported in this work were carried out by means of the full-potential linearized augmented plane wave (FLAPW) method using WIEN2K computer package [18]. Following this approach the space is divided into an interstitial region (IR) and non overlapping (MT) spheres centered at the atomic positions. In the IR region, the basis set consists of plane waves.

Inside the MT spheres, the basis sets is presented by radial solutions of the one particle Schrödinger equation (at fixed energy) and their energy derivatives multiplied by spherical harmonics. The exchange correlation (XC) effects for the structural properties are treated by the local density approximation (LDA) with exchange correlation factor presented in the Ref. [19]

To achieve energy eigenvalues convergence, the wave functions in the interstitial region were expanded in plane waves with a cut-off $K_{max} = 9/R_{MT}$, where R_{MT} denotes the smallest atomic sphere radius and Kmax gives the magnitude of the largest K vector in the plane wave presentation. The valence wave functions in side the spheres are expanded up to l_{max}=10 while the charge density was Fourier expanded up to G_{max}=14. The self-consistent calculations are considered to be converged when the total energy of the system is stable within 10^{-4} Ry. The integrals over the Brillouin zone are performed up to 380 ***k***-points in the irreducible Brillouin zone (IBZ).

Broadening is taken to be 0.04 eV. Our optical properties are scissor corrected by 0.40 eV. This value is the difference between the calculated (2.80 eV) and measured (3.20 eV) energy gap (see Fig. 1). This could be traced to the fact that LDA calculations usually underestimate the energy gaps. A very simple way to overcome this drawback is to use the scissor correction, which merely makes the calculated energy gap equal to the experimental gap.The principal results of the calculations are presented in the Table 1. One can see that the largest values of hyperpolarizabilities and susceptibilities were obtained fro xxx tensor components. A little bit less are the corresponding values for the zxx and xzz components. However, Lorentz local field factor, which is a bridge between the microscopic hyperpolarizabilities and the macroscopic susceptibilities, plays a crucial role. In the investigated crystals there exist a substantial difference between the relative values of hyperpolarizabilities and suscpeptibilities, in particularly for the y-containing tensor components. This may stimulate a possibility to enhance the corresponding susceptibilities by applying of external vectorial fields, in particular of the additional alignment of particular out-of-plane fragments.

Table 1. Calculated values of the second order hyperpolarizabilities and second order susceptibilities for the wavelengths 1064 nm for different tensor components. For the DFT and TDDFT the results correspond to the first order hyperpolarizabilites in the atomic units. For the FLAPW methods all the data correspond to the second order optical susceptibilities in pm/V. The values of the state dipole moments are given in the Debye.

Method	**xxx**	**xyy**	**xyy**	**yyy**	**zxx**	**xyz**	**zyy**	**xzz**	**yzz**	**zzz**	μ_x	μ_y	μ_z
DFT	9382	109	3.30	58	6645	83	24	4962	22	4198	5.64	5.55	1.38
TDDFT	8512	126	4.65	1.06	6800	91	32	5200	18.75	4400	5.89	5.06	1.13
FLAPW	2.21	0.82	0.02	0.05	1.72	0.1	0.08	1.62	0.12	0.16	5.97	5.12	1.38
FLAPW + dc field along c	3.13	0.80	0.18	0.03	1.56	0.12	0.11	1.53	0.25	0.18	6.74	5.03	1.47
FLAPW + dc field along b	1.98	0.89	0.29	0.13	1.21	0.18	0.29	1.87	0.36	0.42	5.12	5.89	1.67
FLAPW + dc field along a	2.89	0.89	0.31	0.34	1.12	0.16	0.31	1.56	0.29	0.24	5..98	5.12	1.06

The performed study reveals that these crystalline systems have very large first order hyperpolarizabilities and possess a great potential to be used for NLO devices. Additional enhancement may be achieved during applications of the dc-electric field along the z axes. The transfer of a proton from 3-nitrophenol to 3-nitroaniline will tend to increase the molecular hyperpolarizabilities of these components in the 3-NA: 3-NPh complex crystal relative to the values of the corresponding neutral molecules.

Following the presented data one can see that for the investigated crystal there exists an additional possibility to enhance their non-linear optical properties by applying of external fields, for example polarized light which may form additional alignment of the crystals. At the same time one can expect substantial anisotropy of the obtained dependences.

4. Results and discussion

4.1. Group theory symmetry analysis

According to the powder X-ray data, the studied crystal is crystallized in orthorhombic space group $Pca2_1$. For the factor group analysis, the unit cell containing four translational non-equivalent 3-NA and 3-NPh units (Z_B=4 – with point group symmetry C_{2v}) was used. Following this reason and applying the site group analysis proposed by Rousseau et al [20,21] , it is possible to carry out the irreducible representation at the center of the Brillouin zone. The optical phonon modes are classified by the group irreducible representations as : $92A_1+93A_2+92B_1+92B_2$. The three acoustic modes ($A_1+B_1+B_2$) were subtracted from the total number of remaining 369 optical modes. In accordance with the selection rules the vibrations of A_2 symmetry are non-active in the IR absorption. From the whole set of optically active 372 modes 348 may be related to inter-molecular and 24 to the crystal lattice vibrations. The details of factor group analysis and correlation scheme for 3-NA and 3-NPh are summarized in Tables 2, 3 and 4 respectively.

Table 2. Summary of factor group analysis of 3-NA : 3-NP

Factor group species C_{2v}	$C_6H_6N_2O_2$ 3-NA C_1 site		$C_6H_5NO_3$ 3-NPH C_1 site		C C_1 site	H C_1 site	N C_1 site	O C_1 site	Optical modes	Acoustic modes
	Internal modes	External modes	Internal modes	External modes	3-nitroanilinium 3-nitrophenolate C_1 site					
A_1	42	3T, 3R	39	3T, 3R	36	30	33	9	93	01
A_2	42	3T, 3R	39	3T, 3R	36	30	33	9	93	0
B_1	42	3T, 3R	39	3T, 3R	36	30	33	9	93	0
B_2	42	3T, 3R	39	3T, 3R	36	30	33	9	93	02
Total modes	168	12T, 12R	156	12T, 12R	144	132	36	60	372	03

Table 3. Correlation scheme for 3-nitroaniline

Free ion Symmetry **C_s**	Site symmetry **C_1**	Factor group symmetry **C_{2v}**	Activity **Raman**	**IR**
84A′		$42A_1$	$\alpha_{xx}, \alpha_{yy}, \alpha_{zz}$	.....
		$42A_2$	α_{xy}	z
	168A	$42B_1$	α_{xz}	.....
		$42B_2$	α_{yz}	x, y
84A″				

Table 4. Correlation scheme for 3-nitrophenol

Free ion Symmetry **C_s**	Site symmetry **C_1**	Factor group symmetry **C_{2v}**	Activity **Raman**	**IR**
78A′		$39A_1$	$\alpha_{xx}, \alpha_{yy}, \alpha_{zz}$	.....
		$39A_2$	α_{xy}	z
	156A	$39B_1$	α_{xz}	.....
78A″		$39B_2$	α_{yz}	x, y

4.2. Phonon mode descriptions

The polarized Raman spectra were recorded in the following Porte configurations: *y*(*xx*)*y*, *y*(*xz*)y and *z(xy)z* the corresponding data are presented in Figs. 3(a) – 3(c), respectively.

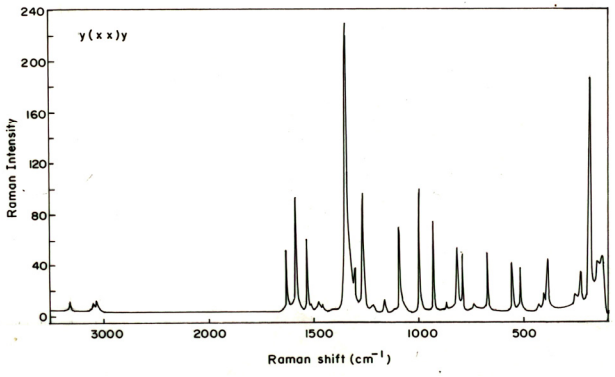

(a)

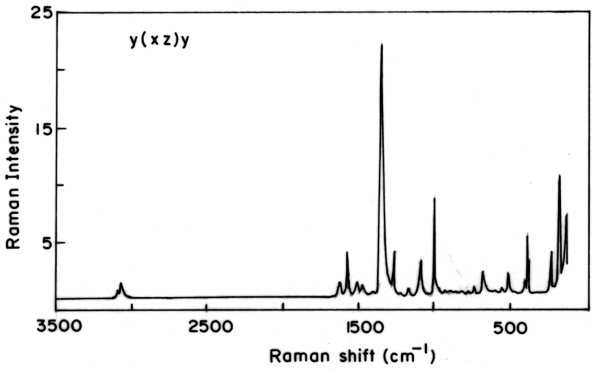

(b)

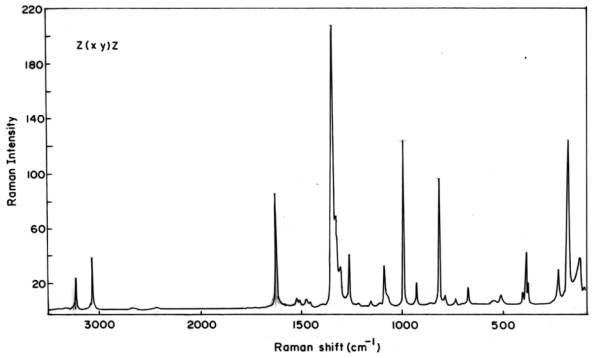

(c)

Fig. 3. (a) Polarized Raman spectrum of 3-NA: 3-NPh crystal in y(xx)y orientation, (b) Polarized Raman spectrum of 3-NA: 3-NPh crystal in y(xz)y orientation, (c) Polarized Raman spectrum of 3-NA: 3-NPh crystal in z(xy)z orientation.

Meredith and Marder [22,23] have proposed methodology to overcome the symmetry problem in the crystallization of ionic salts. This approach has been demonstrated to be a promising strategy for engineering the molecules into noncentrosymmetric alignment by virtue of complexation with a variety of central ions. We may note that the intermolecular hydrogen bonding network formed between amino hydrogen atoms of a cation of an ion pair and phenolate oxygen atoms of adjacent anions of another ion pair are interesting features and play an important role to achieve noncentrosymmetric structures in the present crystals. However, from the presented data it is difficult to establish direct relation between phonon modes and nonlinear optical susceptibilities. The observed optical phonon modes are assigned and depicted in Table 5.

Table 5. Vibrational assignments of 3-NA: 3-NPh.

Polarized Raman (cm^{-1})			IR (cm^{-1})	Symmetry	Assignments
y(xx)y A_1	y(xz)y B_1	z(xy)z A_2			
3313vw	-		3328 s	A_1	$\nu_{as}(NH_3^+)$
-	-	3253 w	3205 w	A_2	$\nu_{as}(NH_3^+)$
3098 vw	3080 vvw	3075 vw	3082 w	$A_1 + B_1 + A_2$	$\nu_s(NH_3^+]$
3075 vw 3080 vw			-	A_1	$\nu_s(NH_3^+)$
-	-	-	2927	-	Overtones and combinations
-	-	-	2435	-	Overtones and combinations
-	-	-	2357	-	Overtones and combinations
-	-	-	1746 w	-	ν_{as}(C-O)
-	-	-	1699 vw	-	$\delta_{as}(NH_3^+)$

Polarized Raman (cm^{-1})			IR (cm^{-1})	Symmetry	Assignments
1626 m	-	1625 ms	1624 s	$A_{1+}A_2$	$\delta_{as}(NH_3^+)$
1584 ms	1580 vw	-	-	$A_1 + B_1$	$\nu_{as}(NO_2)$
1532 ms 1515 vw	1510 vvw	-	1519 vs	$A_1 + B_1$	$\delta_s(NH_3^+)$, $\nu_{as}(NO_2)$, δ(C-N-H) ν(C-C)
1478 vw 1460 vvw	1480 vvw	-	-	$A_1 + B_{1+}A_2$	δ(C-H), ν(C-C)
1348 vs	1350 vs	1352 vs	1342 vs	$A_1 + B_{1+}A_2$	$\delta_{in\ plane}$(C-OH)
1312 w	-	1334 vvw 1312 vvw	-	$A_1 + A_2$	ν(C-C), $\delta_{\ in\ plane}$(C-H)
1260 ms	1260 w	1265 w	1260 ms	$A_1 + B_{1+}A_2$	δ(N-H), ν(C-O)
1217 w	-	-	-	A_1	δ(C-H)
1163 vvw	-	1162 vvw	-	$A_1 + B_{1+}A_2$	ν(C-NO_2), ν(C-O), $\rho(NH_3^+)$
1091 ms	1090 w	1091 w	1077 ms	$A_1 + B_{1+}A_2$	$\delta_{in\ plane}$(C-H), φ ring
997 ms	975 m	996 s	996 ms	$A_1 + B_{1+}A_2$	ν(C-C)
931 ms	931 vvw	931w	927 vw	$A_1 + B_{1+}A_2$	$\delta_{out\ of\ plane}$(C-OH)
867 w	-	-	869 ms	$A_1 + B_1$	$\delta_{out\ of\ plane}$(C-H)
807 m	-	818 ms	809 ms	$A_{1+}A_2$	γ(C-N-H)
793 w	-	791 vvw	-	$A_{1+}A_2$	$\delta_{out\ of\ plane}$(C-H)
738 vw	738 vvw	737 vvw	735 ms	$A_1 + B_{1+}A_2$	γ(C-C-C)
674 w	675 w	675 vvw	667 ms	$A_1 + B_{1+}A_2$	$\delta_{in\ plane}$(C-C-C)
554 w	-	-	539 ms	A_1	δ(C-C-O)
404 ms	-	405 vvw	-	$A_{1+}A_2$	$\omega(NO_2)$
386 ms	385 w	386 ms	-	$A_1 + B_{1+}A_2$	$\delta_{in\text{-}plane}$(C-NO_2)
254 w	-	-	-	A_1	$\tau(NH_2)$
229 w	229 w	228 vw	-	$A_1 + B_{1+}A_2$	Lattice vibrations, $\delta_{out\ of\ -plane}$(C-NO_2)
180 s	177 ms	178 s	-	$A_1 + B_{1+}A_2$	Lattice vibrations
-	146 w	-	-	B_1	Lattice vibrations
-	124 ms	-	-	B_1	Lattice vibrations, $\tau(NO_2)$

vs, very strong; s, strong; ms, medium strong; m, medium; w, weak; vw, very weak; vvw, very very weak.
$\nu_{as,}$ Asymmetric stretching; $\nu_{s,}$ Symmetric stretching ; δ, Deformation; γ, Ring breathing; τ, Torsion; ρ, Rocking; ω, Wagging.

The importance of hyper-conjugative interaction and electron density transfer from lone electron pairs of the Y atom to the X-H anti -bonding orbital in the X-H…..Y system have been analyzed. The intermolecular N-H……..O hydrogen bonding is formed due to the overlap between n(O) and σ*(N-H) which results in stabilization of H-bonded systems. The ammonium group NH_3^+ exists with pyramidal C_{3v} symmetry in free state. Its normal modes of vibrations are $\nu_1(A_1)$, $\nu_2(A_1)$, $\nu_3(E)$ and $\nu_4(E)$. All vibration modes are both IR and Raman active [24,25]. The uncharged amino group has stretching frequencies between 3500 and 3300 cm^{-1} while the charged species are manifested in the spectral range 3300–2500 cm^{-1}. In the title complex, the doubly degenerated asymmetric stretching and bending modes $\nu_3(E)$ and $\nu_4(E)$ are split. The width and fine structure are explained by the large anharmonicity and strong coupling of ν(N-H) stretching with the ν(N-H……O) (also called hydrogen bond strain) and the other intermolecular interactions of the chain. Further this N-H stretching frequency is red shifted in IR, which indicates the weakening of the N-H bond resulting in proton transfer to the neighboring hydrogen. The two medium intensity bands at 3328 cm^{-1} and 3205 cm^{-1} appearing as a doublet in the infrared spectrum and the Raman phonon modes at 3313 cm^{-1} and 3253 cm^{-1} with a weak intensity in the recorded geometries are due to the NH_3^+ asymmetric stretching mode. The strong band at 1624 cm^{-1} and a shoulder at 1699 cm^{-1} in IR are attributed to NH_3^+ asymmetric deformation mode $\nu_4(E)$. This mode is seen as a very weak mode in the *xx* and *xy* orientation of the crystal. These are due to the extensive hydrogen bonding of the crystal. The NH_3^+ symmetric stretching $\nu_4(A_1)$, and bending $\nu_2(A_1)$ modes are identified as medium intensity band at 3082 cm^{-1} and a strong mode at 1519 cm^{-1} respectively in the infrared spectra of the investigated crystal. A very weak optical phonon mode of this vibration is seen in the polarized Raman spectra along *xx* and, *xz* orientations and absent in *xy* orientation due to the stretching and deformational modes of NH_3^+ group. It is obvious that a modification of charge transfer axis, i.e., a vibrational phonon mode displacing the atoms in the direction of charge transfer axis will result in large change in polarizability. In contrast a displacement of atoms in direction where no conjugation is present will have only a small influence on the polarization in that direction. These spectra may indicate that the main tensor components contributions to b tensors should have xxx, zzz, zxx and xzz symmetries. This may be also explained from general structure (see Fig. 1 c). However, it is difficult to find simple relation between the Raman and IR features and the particular optical susceptibilities.

The phenyl ring mode manifests weak bands in the polarized Raman spectra at 1580 cm^{-1}. The intensity of this mode is dependent on the algebraic difference of the electronic effects of the substituents. The strong bands observed at 1519 cm^{-1}in IR and very weak bands around 1510 - 1530 cm^{-1} are attributed to the Kekule C-C stretching mode. These vibrations are expected to interact with C-H in plane bending hydrogen and its carbon moving oppositely but the substituents are nearly motionless [26]. The simultaneous IR and Raman phonon activation of phenyl ring modes provides evidence for the charge transfer interaction between the donor and the acceptor group through the π system leading to β enhancement responsible for NLO activity. The mixing of NO_2 vibrations is also possible in this region.

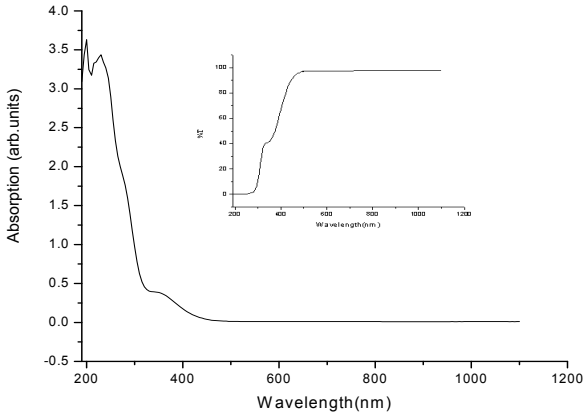

Fig. 4. Optical transmission and absorption spectra of 3-NA: 3-NPh

The presence of phenolate ions in the cocrystallized 3-nitroaniline and 3-nitrophenol single crystal structures is reflected in the highly mixed bands of the C-O stretch, C-OH in-plane deformation together with C-OH out-of-plane bending vibrations. The presence of such groups may indicate on an existence of great potential to enhance the corresponding optical susceptibilities by application of external dc-electric field. The intensity of C-O group bands can increase due to conjugation or formation of hydrogen bonds. The $\nu_{C\text{-}O}$ band is very sensitive to the environment and causes a red shift upon complex formation. Also the C-O phonon modes are very strong and intense found at 1342 cm^{-1} and 1350 cm^{-1} in the infrared and Raman spectrum respectively. A weak optical phonon mode at 1312 cm^{-1} is also seen in the *xx* and *xy* scattering geometries of polarized Raman spectra, blended with N-H deformation at 1260 cm^{-1}. The in phase displacement of hydrogen atoms changes the electronic environment for the donor and acceptor of the chromophores and therefore the polarizability is modified in polarized Raman spectra. In C-O…..H hydrogen bond a charge transfer from the lone pairs of the electron is directed mainly to the anti-bonding orbital in the remote part of the complex. This primary effect of elongation is accompanied by a structural reorganization of the of the proton donor leading to a contraction of the C-O….H bond. Hence this bond is considered as improper hydrogen bond or blue shifting bond. This is ascertained by the presence of in-plane and out-of plane deformation of C - OH occurs at 1342 cm^{-1} and 926 cm^{-1} , respectively as strong bands in the IR and polarized Raman spectra for all

the recorded orientations. This observation provides further evidence that the 3-nitrophenolate ions rather than 3-nitrophenol or the protonated species are present in the cocrystal, since protonation would occur on the carbonyl oxygen. The mechanism of charge separation and radical ion formation can contribute to the molecular mechanism of NLO susceptibilities.

The hydrogen bond modes occur at low frequency region between 50 and 300 cm^{-1}. The low wavenumber hydrogen bond vibrations are generally found to be weak, broad and asymmetric in the Raman spectrum. The low wavenumber degrees of freedom such as librations, induced inter molecular interactions give rise to additional absorption and Raman optical phonon modes and that frequently overlap with the bands of the hydrogen bond modes. The occurrence of intense Raman band in the low frequency region corresponds to NH…….H(O) bond hydrogens and are named as ionic hydrogen bonds through which the charge transfer can take place inside the crystal making the molecule more non linear optical active. The optical phonons at 180 cm^{-1} in the on diagonal geometries of Raman can be assigned to the translational motion of the hydrogen bond. The low frequency lattice modes are stronger in intensity than other modes.

Despite several indications of the charge transfer which is manifested in the polarized Raman modes it is difficult to find a simple rule which relates the polarized Raman spectra with the measured nonlinear optical susceptibilities. However, some opportunities for enhancement of corresponding susceptibilities can be achieved by application of external dc-field.

4.3. Optical transparency

UV-Visible technique can be very helpful in the investigation of NLO materials making it possible to check, both NLO responses and also spectroscopic absorbance in the appropriate wavelength range. Therefore, the wavelengths obtained by UV-Visible spectral analysis can be helpful in planning the synthesis of only the promising NLO materials [27]. It is also necessary to shorten the cut-off wavelength of transmission in the design aspect of NLO materials. As seen in the spectra given in the Fig.4, there is no an absorption in the visible region of the studied compound, i.e. the compound remains transparent in the visible region. The absence of the absorption in the entire visible region might enable the achievement of microscopic NLO response with non-zero values [28]. The β values computed here might be correlated with the UV visible spectroscopic data in order to clarify the molecular structure NLO property relationship in view of a future optimization of the microscopic NLO properties of the investigated compounds. The studied charge transfer complex exhibits slight bathochromic behavior around 300nm which is generally considered as an indicative of molecular second order hyperpolarizibilities with non zero values. Electron donor-acceptor groups are of particular interest because a donor group can provide additional electrons into the π conjugated system leading to a strong interaction from a donor acceptor combination.

4.4. Second harmonic generation

We have performed study of the effective second order optical susceptibility for the fundamental wavelength 1320 nm. Such choosing of 1320 nm wavelength is caused by a fact that total absorption for doubled frequency red 660 nm wavelength is less than for green 530 nm. For this reason we have used the pulsed 10 ns Nd-YAG laser with peak power about 1 MW, pulse repetition about 10 Hz. The investigated crystals were cut in three principal crystallographic planes – ab, bc and dc. Their thickness were varied within 20 μm - 300 μm. The investigated crystals were illuminated by the fundamental wavelength. They were rotated to find the maximal output doubled frequency signal. The later one was detected by the fast-response photodetector connected with the 3 GHz oscilloscope. The interference red filter at 660 nm was used for the spectral separation of the second harmonic generation with respect to the fundamental IR beam. We have used the KDP crystal as a reference of determination of the second order susceptibilities. The better output signal of the SHG was achieved for the polarization of the fundamental laser beam directed in the y direction and for the laser polarization 10-20 degree with respect to the crystallographic axes. This one is in a contradiction with the data presented in the Table 1 presenting theoretical simulations. Such discrepancies may be caused by a fact that for the molecular crystals substantial role begins to play intrinsic defect sub-system [30], which may determined principal nonlinear optical effects. The input-output geometry was optimal for s-s polarization (see Fig. 5). Rotating the crystal we have achieved an enhancement of the SHG (see Fig. 5 a). The behavior of the SHG for the different geometries are presented in the Fig. 5 b. The effective strength of electric field caused by UV-illumination was below 60V/μm. So the main reason of the use of the UV-induced light was to operate by photocharging of the intrinsic defect states. The latter form anisotropic boucle of the defects which are sensitive to the polarization of external light. Generally the results in the Table 1 are substanitlaly overestimated with respect to the experimental data , which may reflect the limitation of the traditional methods of the optical suscpetiblities determinations in the case of the molecular crystals where there are large differences between the intra-molecular and inter-molecular forces. Additionally the moelcualr crystals due to such differences of the chemical bonds favour formation of a larege number defect states, which may be charged under influence of external polarized UV light hitting below the energy gap.

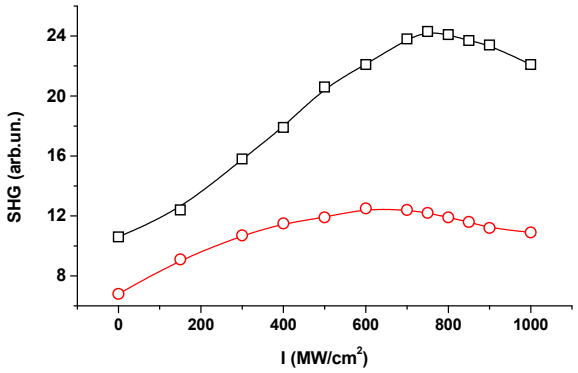

(a)

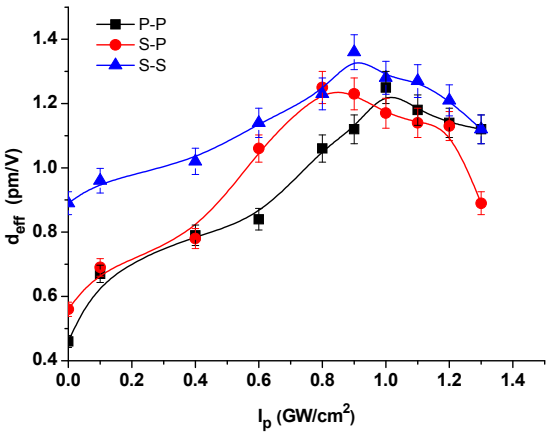

(b)

Fig. 5(a). Dependence of the SHG geometry for UV light polarized parallel to z axes (squares) and perpendicular to the z-axes (rings). The experiment is performed for s-s geometry and the polarization of the incident fundamental line corresponding to optimal geometry. (b). Dependence of the second order optical susceptibilities for the different geometries of the SHG experiment versus the UV-induced power densities.

We have found that that maximal second order susceptibilities was observed for S-S input-output light polarizations achieving value about 0.9 pm/V. The corresponding second order optical susceptibilities achieve the maximal values within the 1.2-1.4 pm/V. Comparison with the theoretical data indicates a fact that the architecture of particular molecule is very far from optimal. So using the UV-induced polarized light one can enhance substantially the second harmonic generation output due to formation of the UV-stimulated local dc-electric field as in the case of the electric-field induced SHG. Following the three different geometries we have obtained a huge anisotropy of the observed second harmonic generation which confirms the observed anisotropy of the Raman spectra. This anisotropy may be related to the defect anisotropy.

We have established that local thermoheating following the laser pyrometers do not exceed the 2-3 degree, which exclude additional anharmonic phonon mechanisms and the Kerr effect contribution is below the precision of the measurements. So one can expect that a UV-induced field effect is prevailing similarly to the UV-simulated charging of the defect trapping levels below the energy gap.

5. Conclusions

A charge transfer complex of 3-nitroanilinium 3-nitrophenolate salts was found to be new second order NLO material having a short cutoff wavelength within UV region. The structural, vibrational and second-order nonlinear optical properties of the crystals were studied under application of the polarized UV-induced field. Besides the ab initio quantum chemical calculations have been performed at HF/6-31G (d) and time dependent DFT method level to derive first order hyperpolarizability. To compare an influence of the crystalline long-range ordering and of the applied effective electric field additional calculations were performed for second order susceptibilities within the FLAPW method. Comparing the values of the second order optical susceptibilities and of the first order hyperpolarizabilites we have established that the principal role in the such kinds of the effects is played by the intrinsic defect states demonstrating substantial anisotropy of the charged trapping levels. We have found that the maximal changes in second order optical susceptibilities were observed during application of the external laser light directed along the z-crystallographic axes which is in a contradiction with the calculations performed in the assumption of the traditional bulk crystals.

Acknowledgement

The authors (R.N) is thankful to Council of Scientific and Industrial Research(CSIR), Government of India, New Delhi for the award of Senior Research Fellowship and V.Krishnakumar is thankful to Indian National Science Academy (INSA), New Delhi and Polish Academy of Science, Poland for the award of fellowship under bilateral Exchange program. One of the authors (K.O.) would like to thank to Polish Science Foundation award (2008) for young scientists.

References

[1] S. J. Lalama, A. F. Garito, Phys. Rev. A. **20**, 1179 (1979).
[2] A. C. Albrecht, A. Morell, Chem. Phys. Lett. **64**, 46 (1979).
[3] D. R. Kanis, M. A. Ratner, T. J. Marks, Chem.Rev. **94**, 195 (1994).
[4] J. Pecaut, R. Masse, J. Mater. Chem. **4**, 1851 (1994).

[5] Cara. C. Evans, M. Bagieu- Beucher, Rene Masse, Jean Francois Nicoud, Chem. Mater. **10**, 847 (1998).
[6] K. S.Huang, D. Britton, M. C. Etter, S. R. Byrn, J.Mater.Chem. **7**, 713 (1997).
[7] M. C. Etter, G. M. Frakenbach, D. A. Adsmond, Mol. Cryst. Liq. Cryst. **187**, 25 (1990).
[8] J. N. Sherwood, Pure Appl.Opt. **7**, 229 (1998).
[9] S. Gunasekaran, M. N.Ponnusamy, Cryst. Res. Technol. **41**, 130 (2006).
[10] J. L. Oudar, J. Zyss, J. Phys. Rev. A. **26**, 2016 (1982).
[11] B. J. Orr, J. F. Ward, Mol. Phys. **20**, 513 (1971).
[12] M. J. Frisch, G. W. Trucks, H. B. Schlegel, G. E. Scuseria, M. A. Robb, J. R. Cheeseman, V. G. Zakrzewski, J. A. Montgomery, Jr.,R. E. Stratmann, J. C. Burant, S. Dapprich, J. M. Millam, A. D. Daniels, K. N. Kudin, M. C. Strain, O. Farkas, J. Tomasi, V. Barone, M. Cossi, R. Cammi, B. Mennucci, C. Pomelli, C. Adamo, S. Clifford, J. Ochterski, G. A. Petersson, P. Y. Ayala, Q. Cui, K. Morokuma, D.K.Malick, A.D. Rabuck, K. Raghavachari, J.B. Foresman, J.Cioslowski, J. V. Ortiz, A.G. Baboul, B. B. Stefanov, G. Liu, A. Liashenko, P. Piskorz, I.Komaromi, R. Gomperts, R. L. Martin, D. J. Fox, T. Keith, M. A. Al-Laham, C. Y. Peng, A. Nanayakkara, C. Gonzalez, M. Challacombe, P. M. W. Gill, B. Johnson, W. Chen, M. W. Wong, J. L. Andres, C. Gonzalez, M. Head-Gordon, E. S. Replogle, J. A. Pople, GAUSSIAN 98, Revision A.7, Gaussian Inc., Pittsburgh, PA, 1998.
[13] D. A. Kleinman, Phys. Rev. **126**, 1977 (1962).
[14] A. Schafer, H. Horn, R. Alrids, Journ.Phys.Chem., **V.97**, 2571 (1992),
[15] T. H. Dunning, Journ. Phys. Chem, **3**, 2825 (1970),
[16] S. J. A. van Gisbergen. Molecular response property calculations using TDDFT in Chemistry. Vrije University, Amsterdam, 1998, p.190
[17] M. Makowska-Janusik, I.V.Kityk, Spectrochimica Acta, **A65**, 511 (2006),
[18] P. Blaha, K. Schwarz, G. K. H. Madsen, D. Kvasnicka , J. Luitz, WIEN2k, An augmented plane wave plus local orbitals program for calculating crystal properties, Vienna University of Technology, Austria (2001).
[19] J. P. Perdew , A. Zunger, Phys. Rev. **B 23**, 5048 (1981).
[20] H. Reis, M. G. Papadopoulos, C. Hattig, J. G. Angyan, R. W. Munn, J. Chem. Phys. **112**, 6161 (2000).
[21] Rousseau, R.P. Bauman, S.P.S. Porto, J. Raman Spectrosc. **10**, 253 (1981).
[22] G. R. Meredith, in Nonlinear Optical Properties of Organic and Polymeric Materials, D. J. Williams, Ed.; ACS Symp. Ser. 233; American Chemical Society: Washington, DC, 1983.
[23] S. R. Marder, J. W. Perry, W. P. Schaefer, Science. **245**, 626 (1989).
[24] K. Nakamoto, Infrared and Raman Spectra of Inorganic and Coordination Compounds, Fifth Edition, Part A, John Wiley & Sons Inc., New York, 1997.
[25] S. D. Ross, Inorganic Infrared and Raman Spectra, Mc Graw-Hill, London, 1972.
[26] N. B. Colthup, L. H. Daly, S. E. Wiberley, Introduction to Infrared and Raman Spectroscopy, Academic Press, New York, 1964.
[27] J. Kulakowska, S. Kucharski, Eur. Poly. J. **36**, 1805 (2000).
[28] S. G. Prabhu, P. M. Rao, S. I. Bhat, V. Upadyaya, S. R. Inamdar, J. Cryst. Growth. **233**, 375 (2001).
[29] Ts. Kolev, I. V. Kityk, J. Ebothe, B. Sahraoui. Chemical Physical Letters, **443**, 309 (2007).
[30] I. V. Kityk, B. Marciniak, A. Mefleh. J. of Physics D: Applied Physics. **34**(1), 1 (2001).

*Corresponding author: vkrishna_kumar@yahoo.com